Salicylic acid 3-hydroxylase regulates *Arabidopsis* leaf longevity by mediating salicylic acid catabolism

Kewei Zhang[a,b], Rayko Halitschke[c], Changxi Yin[a], Chang-Jun Liu[b], and Su-Sheng Gan[a,d,1]

Departments of [a]Horticulture, [c]Ecology and Evolutionary Biology, and [d]Plant Breeding and Genetics, Cornell University, Ithaca, NY 14853; and [b]Brookhaven National Laboratory, Upton, NY 11973

Edited by Richard A. Dixon, University of North Texas, Denton, TX, and approved July 24, 2013 (received for review February 11, 2013)

The plant hormone salicylic acid (SA) plays critical roles in plant defense, stress responses, and senescence. Although SA biosynthesis is well understood, the pathways by which SA is catabolized remain elusive. Here we report the identification and characterization of an SA 3-hydroxylase (S3H) involved in SA catabolism during leaf senescence. *S3H* is associated with senescence and is inducible by SA and is thus a key part of a negative feedback regulation system of SA levels during senescence. The enzyme converts SA (with a K_m of 58.29 μM) to both 2,3-dihydroxybenzoic acid (2,3-DHBA) and 2,5-DHBA in vitro but only 2,3-DHBA in vivo. The *s3h* knockout mutants fail to produce 2,3-DHBA sugar conjugates, accumulate very high levels of SA and its sugar conjugates, and exhibit a precocious senescence phenotype. Conversely, the gain-of-function lines contain high levels of 2,3-DHBA sugar conjugates and extremely low levels of SA and its sugar conjugates and display a significantly extended leaf longevity. This research reveals an elegant SA catabolic mechanism by which plants regulate SA levels by converting it to 2,3-DHBA to prevent SA overaccumulation. The research also provides strong molecular genetic evidence for an important role of SA in regulating the onset and rate of leaf senescence.

aging | benzoic acid | disease resistance | NahG | senescence-associated gene

Salicylic acid (SA) (2-hydroxy benzoic acid), a phenolic compound, has been studied for its medicinal use in humans for more than 200 y (1), and its role as a plant hormone in disease resistance, leaf senescence, flowering, and thermogenesis have also more recently been investigated (1, 2). The roles of SA in plant defense and the hypersensitive response (a fast form of programmed cell death) have been intensively investigated (1, 2). Leaf senescence is a slow form of programmed cell death that allows plants to mobilize nutrients released from senescing cells to seeds, storage organs, or actively growing tissues (3, 4). Although the role of SA in leaf senescence and its underlying molecular mechanism have been less studied, there is some evidence that both disease defense and leaf senescence seem to share some components in SA signaling and regulation (5, 6).

Much research has been carried out on SA biosynthesis. There are two SA biosynthetic pathways in plants: the phenylalanine ammonia lyase (PAL) pathway and the isochorismate (IC) pathway; both pathways use the primary metabolite chorismate (7). The chorismate-derived L-phenylalanine can be converted into SA via either benzoate intermediates or coumaric acid through a series of enzymatic reactions involving PAL, benzoic acid 2-hydroxylase, and other uncharacterized enzymes (8). Chorismate can also be converted to SA via isochorismate in a two-step process involving isochorismate synthase (ICS) and isochorismate pyruvate lyase. In *Arabidopsis*, two ICS enzymes, which convert chorismate to isochorimate, have been identified; the IC pathway contributes ~90% of the SA production induced by pathogens and UV light (9, 10).

In plants, SA may undergo biologically relevant chemical modifications such as glucosylation, methylation, and amino acid (AA) conjugation (7). SA has been shown to be converted to SA sugar conjugates SA O-β-glucoside (SAG) and salicyloyl glucose ester by SA glucosyltransferases (11, 12). The SA glycosides are actively transported from the cytosol to the vacuole as an inactive storage form that can later be converted back to SA (13). Methylation inactivates SA but increases SA's membrane permeability and volatility, thus allowing more effective long-distance transport of this defense signal (14). AA conjugation of SA at trace levels was found in infected *Arabidopsis* plants (15). Recently, high levels of 2,3- and 2,5-dihydroxybenzoic acid (2,3-DHBA and 2,5-DHBA, respectively) sugar conjugates were detected in infected or aged *Arabidopsis* leaves, and they seemed to be the major inactive form of SA (16). SA in transgenic *Arabidopsis* plants expressing a bacterial salicylate hydroxylase (encoded by NahG) was shown to be converted to catechol; the *NahG* transgenic plants have thus been useful in plant defense and senescence studies involving SA (17, 18). However, the enzyme(s), presumably SA hydroxylases, responsible for the formation of 2,3- and 2,5-DHBA have not been identified in plants yet. Here we report our discovery and characterization of a unique SA 3-hydroxylase (S3H) that converts SA to 2,3-DHBA, a precursor of SA's major storage form 2,3-DHBA sugar conjugates, and plays a pivotal role in SA catabolism and homeostasis and in regulation of leaf senescence.

Results

***SAG108*/*S3H* Is a Senescence-Associated Gene and Can Be Induced by SA.** At4g10500 was initially identified as a senescence-associated gene called *SAG108* from our previous transcriptomic analyses of leaf senescence in *Arabidopsis* (19) and was found to encode a functional S3H as described herein. RNA gel blot analysis revealed that the *S3H* transcript accumulated in senescing leaves but was barely detectable in nonsenescence leaves, which showed an expression pattern similar to that of a known senescence-associated transcription factor *AtNAP* (Fig. 1*A*) (20). The *S3H* expression was also readily inducible after SA treatment for 6 h, with a similar induction pattern to that of *PR1*, which is well known for its inducibility by SA (Fig. 1*B*) (21).

S3H Regulates Onset and Progression of Leaf Senescence. To investigate the biological function of *S3H*, a transfer DNA (T-DNA) insertion line (SALK_059907) was characterized. This line contains a T-DNA insertion in the second exon of *S3H* that completely abolishes *S3H* expression in homozygous mutant plants as revealed by RNA gel blot analysis (Fig. 1 *C* and *D*). The *s3h* knockout plants exhibited a remarkably accelerated leaf senescence phenotype characterized by lower chlorophyll content and reduced ratio of variable fluorescence to maximal fluorescence (F_v/F_m) compared with those of age-matched WT plants (Fig. 2 *A*–*C* and Fig. S1*B*); however, the early stages of growth and development of the plants that were 25 d after germination

Author contributions: K.Z., C.-J.L., and S.-S.G. designed research; K.Z., R.H., C.Y., and S.-S.G. performed research; K.Z., R.H., C.-J.L., and S.-S.G. analyzed data; and K.Z. and S.-S.G. wrote the paper.

The authors declare no conflict of interest.

This article is a PNAS Direct Submission.

[1]To whom correspondence should be addressed. E-mail: SG288@cornell.edu.

This article contains supporting information online at www.pnas.org/lookup/suppl/doi:10.1073/pnas.1302702110/-/DCSupplemental.

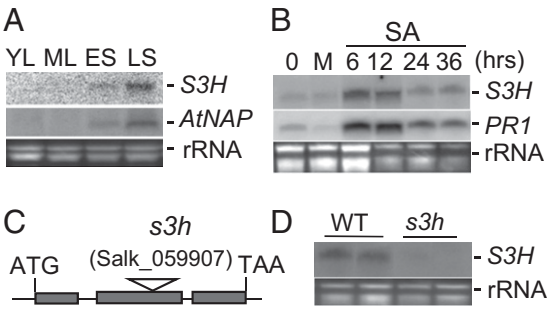

Fig. 1. Senescence-associated and SA-induced expression of *S3H* in WT and in T-DNA insertion line. (*A*) *S3H* was expressed during leaf senescence. ES, early senescence leaves; LS, late senescence leaves; ML, mature leaves; YL, young leaves. *AtNAP*, a senescence marker gene, was used as a positive control. (*B*) *S3H* was induced by SA. The SA-inducible gene *PR1* served as a positive control. 0, leaves without treatment; M, leaves treated with mock solution for 36 h. (*C*) Illustration of T-DNA insertions in line SALK_059907. (*D*) Characterization of T-DNA insertion line of *C* by RNA gel blot analysis of *S3H* expression in the early senescence leaves of WT and the *s3h* mutant plants (*s3h*). Two independently isolated RNA samples were used.

of seeds (DAG) old seemed to be normal (Fig. 3*A* and Fig. S1*A*). The F_v/F_m ratio reflects the activity of photosystem II.

The leaf senescence program in *s3h* mutants was accelerated in two aspects. First, the senescence rate was accelerated. It took 9.5 d on average for senescence to progress from the leaf tip to the petiole in WT but only 2.7 d in the *s3h* leaves (Fig. 2*G*). Second, the onset of senescence was earlier (visible sign of yellowing at the leaf tip); in *s3h* the onset occurred 16.8 d after emergence (DAE) of leaves, compared with 19.2 DAE in WT (Fig. 2*G*). The earlier onset of senescence and the faster senescence progression are also observed from the leaf survival curves (Fig. 2*H*). The *s3h* null mutation is responsible for the phenotype because a construct (pGL3228) carrying an intact S3H (including its promoter region) restored *s3h* to WT (Fig. S1*C*).

In contrast, when *S3H* was constitutively overexpressed in WT under the direction of the cauliflower mosaic virus 35S promoter (Fig. S2), leaf senescence was significantly delayed (Figs. 2 *D–F* and 3*A*), but the flowering time was not altered (Fig. 3*A*). As shown in Fig. 2*D*, leaves of the 45 DAG WT plants had been senescing but leaves of the age-matched *S3H* overexpression transgenic plants remained green. Also, it took 14.6 d for senescence to progress from the leaf tip to the petiole in the S3H overexpression lines (S3HOE) compared with 9.5 and 2.7 d in WT and *s3h*, respectively (Fig. 2*G*). The onset of leaf senescence in S3HOE, which occurred at 21.2 DAE, was also delayed compared with 19.2 DAE in WT and 16.8 DAE in *s3h* (Fig. 2*G*).

Expression of Senescence-Associated Genes and Defense-Related Genes Is Accelerated in *s3h* and Delayed in S3HOE Lines. In addition to the above phenotypic characterization, we performed RNA gel blot analyses of two widely used leaf senescence marker genes, *SAG12* and *SAG13*, and three SA signaling marker genes, *EDS1*, *PAD4*, and *PR1*, in leaves of WT, *s3h*, and S3HOE lines at different ages (Fig. 3*B*). The highly senescence-specific *SAG12* transcripts were readily detectable in the rosette leaves of 35 DAG *s3h* mutant and 40 DAG WT plants but were not detected in the S3HOE1 plants at 40 DAG. Likewise, the *SAG13*, *PR1*, *EDS1*, and *PAD4* were also found to be precociously expressed in the *s3h* mutants but significantly suppressed in the overexpression lines. These data suggest that *S3H* regulates senescence-associated genes and genes involved in SA signaling.

S3H Mediates the Conversion of SA to 2,3-DHBA *in Planta*. The metabolite profiles of SA in young and senescing plants of WT, *s3h*, and S3HOE lines were analyzed using liquid chromatography (LC)–MS/MS. The levels of free SA, SA sugar conjugates, and SA derivatives including 2,3-DHBA and 2,5-DHBA and their sugar conjugates are summarized in Table 1.

The free SA levels in rosette leaves of young or senescing *s3h* mutant plants were 625% and 710% of those of WT, whereas the free SA concentrations in rosette leaves of young or senescing S3HOE1 lines were reduced to only 10–12.5% of those in WT. Similarly, the concentrations of SA glucosides (SAG) in leaves of young or senescing *s3h* mutant plants were also increased to 267% and 317% of those of WT, respectively. However, the SAG levels were reduced to undetectable levels in leaves of both young and senescing S3HOE1 lines (Table 1).

In contrast to SA, the levels of free 2,3-DHBA and 2,5-DHBA, two major catabolites of SA in *Arabidopsis*, were too low to be detected, but the levels of their sugar conjugates were drastically changed. In the *s3h* mutant, free SA and SAG were accumulated to very high levels, as mentioned above. However, the total levels of 2,3-DHBA sugar conjugates (2,3-DHBX + 2,3-DHBG) were not detected in the *s3h* mutant, whereas the total levels of 2,5-DHBA sugar conjugates (2,5-DHBX + 2,5-DHBG)

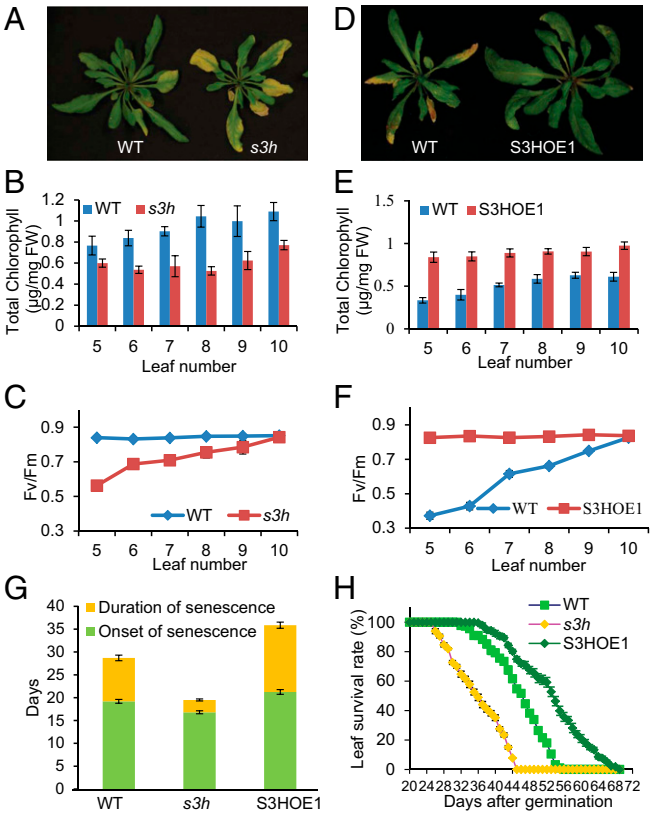

Fig. 2. Phenotypic analysis of *s3h* knockout and *S3H* overexpression lines. (*A*) *s3h* null mutant (*Right*) exhibited an accelerated leaf senescence phenotype compared with WT (*Left*) at 35 DAG. (*B*) Chlorophyll contents in the 5th to 10th leaves (counted from bottom to top with the first the oldest) of WT and *s3h* mutant shown in *A*. Bars show SE, $n = 6$. (*C*) F_v/F_m ratios of leaves of WT and *s3h* mutant shown in *A*. Bars show SE, $n = 6$. (*D*) *S3H* overexpression line 1 (S3HOE1, *Right*) displayed a remarkably delayed leaf senescence phenotype compared with that of WT at 45 DAG. (*E*) Chlorophyll contents of the 5th to 10th leaves from WT and S3HOE1 plant in *D*. Bars are SE, $n = 6$. (*F*) F_v/F_m ratios of leaves of WT and S3HOE1 shown in *A*. Bars show SE, $n = 6$. (*G*) Altered onset and pace of leaf senescence in *s3h* and *S3HOE1* plants compared with those of WT. Green histograms indicate days from leaf emergence to the onset of senescence (visible yellowing at the leaf tip). Yellow histograms indicate the time period (days) it takes for senescence to progress from the first visible yellowing at the leaf tip to the leaf petiole. The sixth rosette leaves were used for the assay. Bars show SE, $n = 6$. (*H*) The survival curve of WT, *s3h* mutant, and S3HOE1 transgenic plants. Bars show SE, $n = 16$.

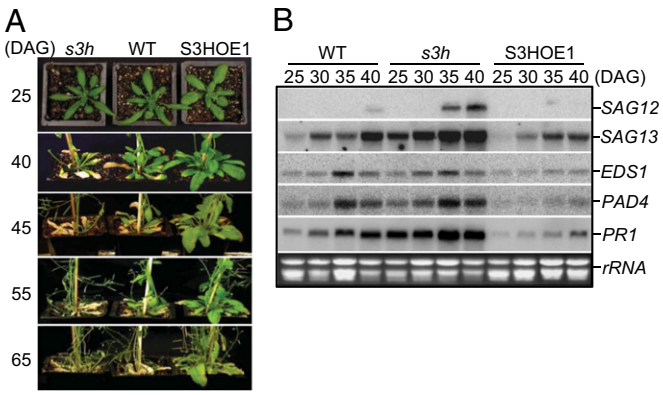

Fig. 3. Phenotypic and transcriptional changes in *s3h* and S3HOE1 plants compared with those of WT. (*A*) Phenotypes of *s3h* mutant, WT, and S3HOE plants at different ages. (*B*) RNA gel blot analyses of expression of senescence-associated genes (*SAG12* and *SAG13*) and SA-responsive genes (*EDS1*, *PAD4*, and *PR1*) in leaves of WT, *s3h*, and S3HOE1 plants at 25, 30, 35, and 40 DAG, respectively. All rosette leaves from two plants at each time point were harvested for RNA extraction.

were increased to 113% and 162% of those of WT in the young leaves and senescing leaves, respectively. By contrast, in the S3HOE1 leaves, the levels of both 2,3-DHBA sugar conjugates (2,3-DHBX + 2,3-DHBG) were significantly increased to 187% and 224% of those of rosette leaves of WT (young or senescing), respectively, but the levels of 2,5-DHBA sugar conjugates (2,5-DHBX + 2,5-DHBG) were significantly reduced to 43% and 40% of those of WT, respectively (Table 1). These data strongly suggest that S3H converts SA to 2,3-DHBA in vivo.

Recombinant S3H Possesses SA 3- and 5-Hydroxylase Activities. Sequence analyses revealed that *S3H* encodes a protein with similarity to the 2-oxoglutarate–Fe(II) oxygenase family enzymes (including a well-known F3H enzyme) that have a conserved catalytic domain Pfam PF03171 (Figs. S3 and S4) (22). Because the above phytochemical analyses implied that S3H catalyzes SA to produce 2,3-DHBA, we performed biochemical analyses to confirm the enzymatic activity using recombinant S3H enzyme overproduced in and purified from *Escherichia coli*. To eliminate nonenzymatic oxidation of SA due to hydroxyl radicals (·OH), catalase was added to each reaction to remove the hydroxyl radicals. The recombinant S3H enzyme converted SA to both 2,3-DHBA and 2,5-DHBA in the presence of ferrous iron, ascorbate, 2-oxoglutarate, and catalase (Fig. 4 *A* and *B*). The 2,3-DHBA and 2,5-DHBA produced by the recombinant S3H have the same retention times and UV spectra as those of the 2,3-DHBA and 2,5-DHBA authentic standards, respectively (Fig. 4 *B–D*). The mass spectra of produced 2,3-DHBA and 2,5-DHBA were also characterized by LC–MS/MS (Fig. 4 *E* and *F*). The enzyme activity increased with the increase of temperature from 4 °C to 40 °C and decreased from 40 °C to 50 °C, suggesting the optimal temperature of this enzyme is approximately 40 °C (Fig. S5*A*). The effect of pH on the enzyme activities was also tested and the optimal pH was 6.0 under our test conditions (Fig. S5*B*). The apparent K_m value for SA of the recombinant S3H was determined to be 58.29 μM at the optimal temperature and pH conditions (Fig. 4*G*). The substrate specificity of the recombinant S3H was also investigated using benzoic acid and anthranilic acid, two chemicals with structures similar to that of SA. The S3H enzyme did not have detectable activity after a 30-min reaction under the same conditions as those for SA (Table S1), suggesting that the recombinant S3H enzyme has high substrate specificity.

Discussion

Our research has revealed a unique negative feedback regulation mechanism by which plants modulate their endogenous SA levels at the onset of and during leaf senescence and has provided strong molecular genetic evidence that S3H, via modulating SA levels, has a pivotal role in controlling leaf senescence.

Elucidation of biosynthesis and catabolism of SA is important for understanding its biological functions. The PAL and IC pathways have been well studied and proposed to be the two main routes responsible for SA biosynthesis (7). However, the catabolism of SA is less understood (7). Our identification and characterization of S3H uncovered a negative feedback regulatory mechanism by which plants regulate SA levels. Briefly, *S3H* is induced by SA, and the induced S3H enzyme in turn hydrolyzes SA to 2,3-DHBA, a deactivated form of SA (16, 23), to prevent overaccumulation of SA.

The feedback regulation is supported by the facts that (*i*) *S3H* is readily induced by the treatment with SA (Fig. 1*B* and Table S2) and (*ii*) *S3H* is highly expressed in senescing leaves (Fig. 1*A*), which is most likely caused by the elevated levels of endogenous SA in senescing leaves (Table 1 and refs. 16 and 24). In senescing leaves of the SA-deficient *NahG* transgenic plants, the expression of *S3H* is almost undetectable, but in the senescing leaves of the jasmonate-deficient mutant *coi1* and the ethylene-signaling mutant *ein2* (as controls) *S3H* expression is not affected (Fig. S6) (25).

The feedback regulation is further supported by the demonstration of S3H's enzymatic activity. Although the recombinant S3H possesses both 3-hydroxylase and 5-hydroxylase activities that convert SA to 2,3- and 2,5-DHBA, respectively, in vitro (Fig. 4), S3H most likely acts as SA 3-hydroxylase in vivo because disruption of *S3H* renders 2,3-DHBA sugar conjugates undetectable, whereas overexpression of S3H leads to a very high level of accumulation of the 2,3-DHBA sugar conjugates (Table 1). In contrast, the levels of 2,5-DHBA sugar conjugates increased in *s3h* and decreased in the overexpression lines (Table 1), presumably resulting from changes in the SA metabolic flux in these mutants. For example, as shown in Fig. 5, because the conversion of SA to 2,3-DHBA is blocked in *s3h*, more SA

Table 1. Analysis of metabolites SA, 2,3-DHBA, and 2,5-DHBA and their sugar conjugates in young and senescing rosette leaves

	Free acids, μg/g FW			Xyloside derivatives, μg/g FW			Glucoside derivatives, μg/g FW		
Genotypes	SA	2,3- DHBA	2,5- DHBA	SAX	2,3-DHBX	2,5-DHBX	SAG	2,3-DHBG	2,5-DHBG
WT(Y)	0.08 ± 0.02	ND	ND	ND	17.32 ± 1.64	14.74 ± 1.05	0.33 ± 0.04	2.06 ± 0.18	0.20 ± 0.07
s3h (Y)	0.50 ± 0.08*	ND	ND	ND	ND	16.52 ± 0.92	0.88 ± 0.12*	ND	0.40 ± 0.11
S3HOE1(Y)	0.01 ± 0.00*	ND	ND	ND	34.14 ± 4.66*	6.34 ± 1.26*	ND	2.11 ± 0.35	0.03 ± 0.03*
WT (S)	0.40 ± 0.1	ND	ND	ND	41.44 ± 4.90	36.35 ± 3.11	0.52 ± 0.09	3.87 ± 0.51	1.24 ± 0.10
s3h (S)	2.84 ± 0.42*	ND	ND	ND	ND	58.00 ± 5.31*	1.65 ± 0.09*	ND	3.00 ± 0.30*
S3HOE1(S)	0.04 ± 0.02*	ND	ND	ND	92.18 ± 9.80*	14.73 ± 1.78*	ND	9.40 ± 1.71*	0.18 ± 0.08*

The data represent the means ± SE of five to six replications.
*Student *t* test, $P < 0.01$, represents significant difference between WT and *s3h* mutant or WT and S3HOE1. 2,3-DHBA, 2,3-dihydroxybenzoic acid; 2,5-DHBA, 2,5-dihydroxybenzoic acid; 2,3-DHBX, 2,3-DHBA xyloside; 2,5-DHBX, 2,5-DHBA xyloside; 2,3-DHBG, 2,3-DHBA glucoside; 2,5-DHBG, 2,5-DHBA glucoside; FW, fresh weight; ND, not detectable: S, rosette leaves from 35-DAG plants; SA, salicylic acid; SAG, SA glucoside; SAX, SA xyloside; Y, rosette leaves from 25-DAG plants.

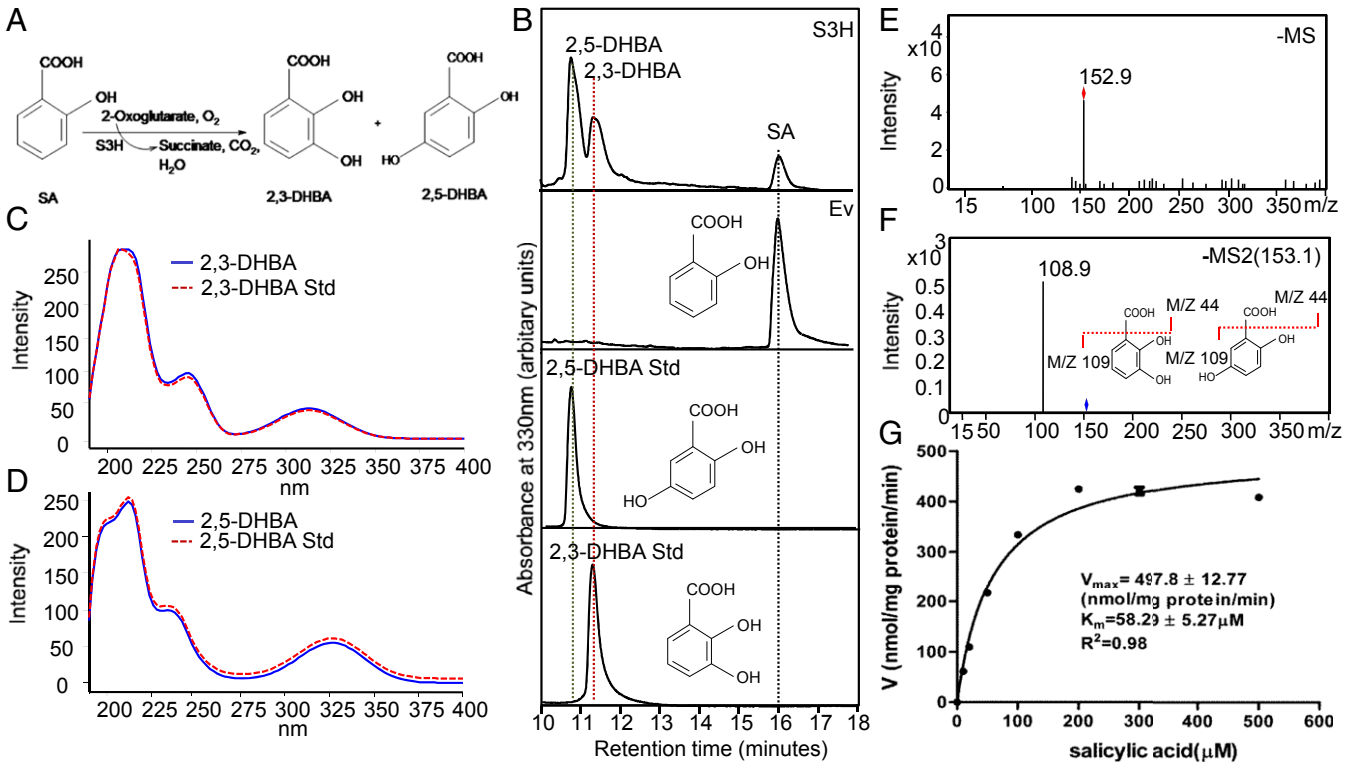

Fig. 4. Conversion of SA to 2,3-DHBA and 2,5-DHBA by recombinant S3H enzyme in vitro. (*A*) Biochemical reaction catalyzed by recombinant S3H in vitro. (*B*) HPLC profiles of 30-min reaction of the recombinant S3H protein and empty vector extracts (Ev) incubated with SA. The authentic 2,3-DHBA and 2,5-DHBA were used as standards. (*C*) The UV spectra of the enzymatic product 2,3-DHBA is identical to that of the 2,3-DHBA standard. (*D*) The UV spectra of the enzymatic product 2,5-DHBA is identical to that of the 2,5-DHBA standard. The S3H enzymatic products 2,3-DHBA and 2,5-DHBA also have the same tandem ESI–mass spectra MS (*E*) and MS2 (*F*), respectively. (*G*) Kinetics of the recombinant S3H (SA as the substrate). The mean and SE are shown, $n = 4$.

becomes available for its conversion to 2,5-DHBA. It has been postulated that 2,3- and 2,5-DHBA species are products of SA oxidation by reactive oxygen species (16). Our research, however, provides direct evidence that 2,3-DHBA is enzymatically synthesized from SA, which enriches our current understanding of SA metabolic pathways, as shown in Fig. 5. Whether 2,5-DHBA is also enzymatically formed needs to be investigated.

Our research reported here also provides strong molecular genetic evidence that *S3H* has a pivotal role in regulating the onset and rate of leaf senescence in *Arabidopsis* by modulating the endogenous levels of SA. *S3H* was initially identified during our leaf senescence transcriptomic analyses (19) as a senescence-associated gene whose transcript levels increase with the progression of leaf senescence (Fig. 1*A*). Leaf senescence was significantly accelerated in the T-DNA insertion *s3h* knockout plants but remarkably attenuated in the S3H overexpression lines (Figs. 2 and 3*A*). Specifically, under our growth conditions, a WT leaf started to senesce (visible sign of yellowing at the leaf tip) at 19.2 DAE and took 9.5 d for the senescence to progress from the tip to the petiole. By comparison, a leaf of *s3h* or *S3HOE* began senescence 2.4 d earlier or 2 d later than that of WT, respectively. The rate of leaf senescence was also 72% faster in *s3h* and 54% slower in *S3HOE* than the rate of WT (Fig. 2G). Consistently, the expression of the leaf senescence marker genes *SAG12* and *SAG13* was also enhanced in *s3h* and inhibited in *S3HOE* (Fig. 3*B*).

S3H regulates leaf senescence most likely by controlling the SA levels. As discussed above, *S3H* modulates the SA levels in plants via a negative feedback regulatory mechanism. The SA levels in the senescing leaves were higher than those in the young leaves (Table 1). Furthermore, the SA levels in *s3h* were much higher than in WT (Table 1). In contrast, the SA levels in S3HOE were much lower (Table 1). Previous correlative studies that revealed low SA levels in young leaves and high concentration in senescing leaves have suggested that SA promotes leaf senescence (26). The suppression of *SAG101*, whose product interacts with PAD4 and EDS1 of SA signaling (27), displayed a delay in leaf senescence (28), also supporting a role of SA in leaf senescence. Overexpression of a bacterial gene named *NahG* reduced the SA levels and delayed leaf senescence, which further supports a role of SA in promoting leaf senescence (24). Our research provides two lines of evidence for SA's role in leaf senescence. One line of evidence comes from S3HOE plants that, like NahG plants, have very low levels of SA (Table 1) and display a significant delay in leaf senescence (Figs. 2*D* and 3*A*). The other line of the evidence comes from *s3h* knockout plants that accumulate high levels of SA (Table 1) and exhibit an early senescence phenotype (Figs. 2*A* and 3*A*). It should be noted that although *NahG*-overexpressing plants have been useful in many studies involving SA, the introduction of the bacterial gene may complicate interpretation of the data. For example, the NahG enzyme converts SA to catechol, which is quite different from the natural metabolites of SA in plants. Therefore, our S3HOE may be a better system for SA-related research in the future.

In addition to leaf senescence, *S3H* seems to have a role in plant defense. Analyses of published (29) and other online microarray data (www.genevestigator.com) revealed that *S3H* can be induced by pathogen infection (Fig. S7 and Table S2). Consistently, the levels of 2,3-DHBA (the product of S3H-catalyzed reaction) derivatives were increased in *Arabidopsis* after challenging with pathogen (16). Knockout and overexpression of this gene resulted in enhanced and reduced resistance to *Pseudomonas syringae* pv. *Tomato DC3000*, respectively (Fig. S8). Further analyses are needed to confirm the role.

Materials and Methods

Plant Materials and Growth Conditions. *Arabidopsis thaliana* ecotype Col-0 was used as WT for all experiments. The T-DNA insertion line SALK_059907

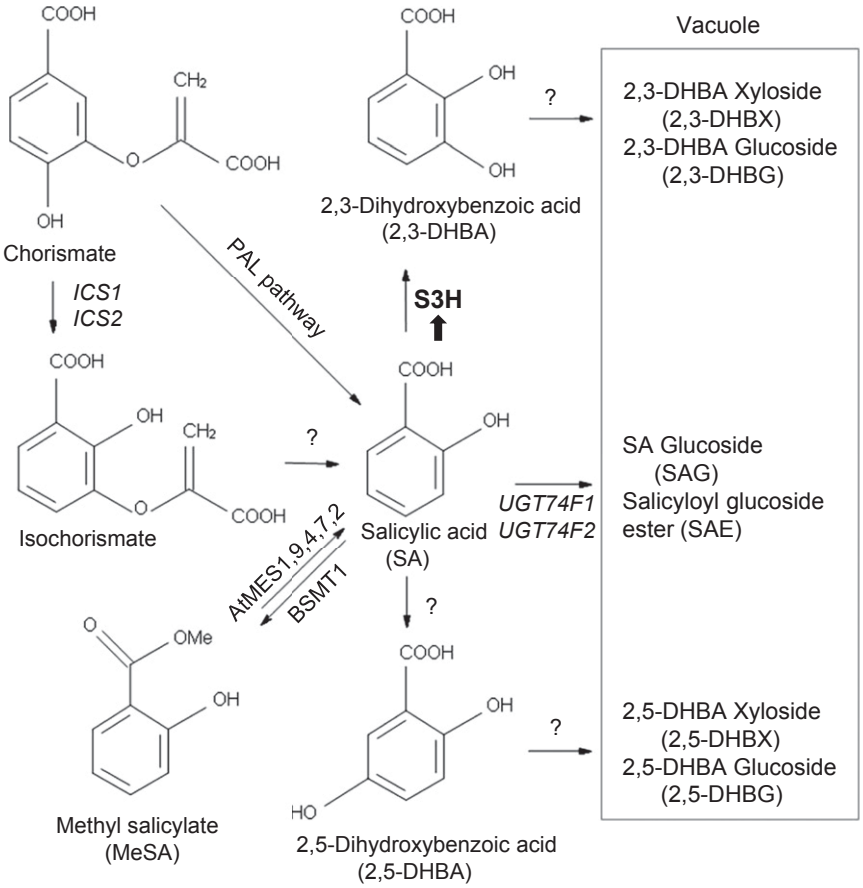

Fig. 5. Proposed SA metabolic pathways enriched with the newly discovered S3H in *Arabidopsis*. The SA 3-hydroxylase (S3H) indicated in bold reported here is induced by accumulating SA (indicated by a black arrow) and it catalyzes the SA to form 2,3-DHBA that will be subsequently conjugated by sugars by unknown enzymes to produce the storage form 2,3-DHBA sugar conjugates. The SA may also be converted to 2,5-DHBA (by an unknown enzyme) that is then converted to its sugar conjugates. In addition, SA can be catalyzed to produce its storage form salicylic sugar conjugates by enzymes UGT74F1 and UGT74F2. The methytransferase BSMT1 is responsible for the production of the functional form methylsalicylic acid from SA and methylesterases 1, 2, 4, 7, and 9 are responsible for the reverse reaction from methylsalicylic acid to SA. Anabolically, two routes including the IC pathway and PAL pathway have been implicated in SA synthesis. In *Arabidopsis* the ICS pathway plays the main role and the PAL pathway plays a minor role, either directly or indirectly, in the production of SA. The ICS1 and ICS2 are responsible for converting chorismate to isochorismate. The enzyme from isochorimate to SA is yet to be discovered.

was obtained from *Arabidopsis* Biological Resource Center (ABRC). Seeds were sown on Petri dishes containing Murashige and Skoog medium with 0.7% (wt/vol) phytoagar and appropriate antibiotics and kept at 4 °C for 2 d before being moved to a growth chamber. Seedlings with two true leaves were transplanted to Cornell mix soils (three parts peat moss:two parts vermiculite:one part perlite). WT, mutant, and/or transgenic plants were grown side by side in the same tray to minimize possible variation of growth conditions. Plants were grown at 22 °C in a growth chamber with 60% relative humidity under constant light (120 $\mu mol \cdot m^{-2} \cdot s^{-1}$ light from a mixture of fluorescent and incandescent bulbs).

Identification of T-DNA Insertion *s3h* Plants. Gene-specific primers G2563, G2564 (all of the primers used in this research are listed in Table S3) and T-DNA left border primer G2325 (LB1) were used to identify homozygous mutant plants of *s3h*.

Chemicals. All chemicals used in this research were purchased from Sigma-Aldrich unless otherwise stated.

SA Treatment. Col-0 plants (25 DAG) were sprayed with 5 mM SA in 0.005% Silwet L-77 (Lehele Seeds) or only 0.005% Silwet L-77 (mock). All rosette leaves of individual plants for RNA extraction were collected at different time points after the spray.

Constructs. The coding sequence of *S3H*, which was PCR-amplified with *S3H*-specific primers G2563 and G2564, was cloned into pGEM-T easy vector (Promega), released with HindIII and PstI, and subcloned to the binary vector pGL800 (30) to form pGL3135, which allows the overexpression of *S3H* in plants. The DNA fragment released from EcoRI digestion of BAC F7L13 DNA (obtained from ABRC) contained the whole *S3H* gene including its promoter region and was cloned into the binary vector pPZP211 at the EcoRI site to form pGL3228 for the complementation of *s3h*. To produce His-tagged S3H recombinant protein, the ORF of *S3H* was PCR-amplified using a pair of primers, S3H_BamHI and S3H_HindIII, and was cloned into pET28a (Novagen) to form pET28a-S3H. All constructs were verified by DNA sequencing.

Chlorophyll Contents, F_v/F_m Assay, and Survival Curves. Chlorophyll was extracted and quantified as described previously (28). Fluorescence in leaves was measured using a portable chlorophyll fluorometer according to the manufacturer's instructions (OS1-FL; Opti-Sciences). The F_v/F_m for each leaf was quantified directly using the fluorometer's test mode 1. The survival curve assay was based on visual observation of leaf yellowing. The completely yellowed leaf was regarded as a dead leaf. The survival rates of WT, *s3h*, and S3HOE1 plants were counted from 20 DAG to 70 DAG.

Transcript Analyses. Total RNA extraction and RNA blot analysis were performed as described previously (28). The DNA templates for probe labeling were amplified by the following different pairs of primers: *S3H*, G2956 and G2957; *AtNAP*, G3149 and G3150; *SAG12*, G10 and G246; *SAG13*, G9 and G16; *EDS1*, EDS1F and EDS1R; *PAD4*, PAD4F and PAD4R; and *PR1*, PR1F and PR1R (Table S3). The ethidium bromide staining of the RNA gels was used to show approximate amount of total RNA loading on each lane.

Transformation. The binary vectors were electroporated into the *Agrobacterium tumefaciens* strain ABI1 and transformed into the WT or *s3h* mutant via the floral dip method (31). Approximately 40 kanamycin-resistant T1 transgenic lines for each transgene were selected. Phenotypic analyses were performed in the T2 generation and confirmed in the T3 generation. Homozygous plants were used in all experiments.

Metabolite Analysis. All rosette leaves of 25 DAG and 35 DAG plants of WT, *s3h*, and S3HOE1 transgenic plants were collected for analysis of free SA, 2,3-DHBA, and 2,5-DHBA using a protocol described previously (32). Ten-microliter extracts were injected for analysis using an LC–MS (Quantum Access; Thermo Scientific) as described (33). The SAG, 2,3-DHBX, 2,3-DHBG, 2,5-DHBX, and 2,5-DHBG samples with internal standard [^{2}H4]SA (CDN Isotopes) were extracted as described previously (34). Glycosides were separated on a C18 reversed-phase column (Gemini-NX, 3 μm, 150 × 4.6 mm;

Phenomenex) and the following solvent gradient (solvent A, 0.1% formic acid in water; solvent B, 0.1% formic acid in acetonitrile): initial 5% B to 75% B at 45 min, and 45–52 min 75% B at a flow rate of 0.2 mL·min^{-1}. The MS detector was equipped with an electrospray ionization (ESI) probe operated under negative ionization conditions: spray voltage 4.0 kV, capillary temperature 360 °C, sheath gas (N_2) pressure 15 arbitrary units, and auxiliary gas (N_2) pressure 10 arbitrary units. Mass spectra were recorded in full scan mode (*m/z* 100 to *m/z* 1,000) to determine molecular ions $[M-H]^-$ used for glycoside quantification. Glycoside identity was verified by comparing UV absorption, retention time, and collision-induced dissociation [CID energy 20 V, CID gas (Ar) pressure 1.5 mTorr] fragmentation of selected molecular ions with published data (16). Five to six biological replicates of each genotype were analyzed.

S3H Recombinant Protein Expression in and Purification from *E. coli*. The construct pET28a-S3H was introduced into *E. coli* BL21 (DE3, pLys3; Invitrogen). The bacterial cells containing pET28a-S3H were induced with 0.5 mM isopropyl β-D-1-thiogalactoside for 24 h at 18 °C and were collected and disrupted by sonication in lysis buffer [20 mM Tris·Cl (pH 7.5), 2 mM EDTA, 2 mM β-mercaptoethanol, 1 mM PMSF, 10 mM imidazole, 0.1% Triton X-100, and 20 mM sodium ascorbate]. All subsequent purification procedures involving His-Bind resin were performed at 4 °C according to the manufacturer (Novagen). The recombinant protein concentration was quantified using Quick Start Bradford Dye Reagent (Biorad). DTT (2 mM) was added to the enzyme solution and the protein was immediately kept in a refrigerator at −80 °C.

Enzyme Assay. The enzyme assay was performed using a method modified from Saito et al. (35). The reaction mixture (100 μL) contained 5 mM DTT, 4 mM sodium ascorbate, 1 mM 2-oxoglutaric acid, 0.4 mM $FeSO_4$, 0.1 mg/mL catalase, 50 mM Tris·Cl (pH 8.0) or other buffer, 8–15 μg recombinant protein, and various concentrations of SA. To determine the optimal temperature and pH for enzyme activity of S3H, the protein was incubated with 200 μM SA substrate in Tris·Cl buffer (pH 8.0) at different temperatures for 15 min or 500 μM SA substrate, in 50 mM sodium citrate, Tris·Cl, and glycine buffers with different pH at 40 °C for 15 min. For enzyme kinetics analysis, various substrate SA concentrations ranging from 10 to 500 μM were used and the incubation proceeded for 6 min with pH 6.0. All of the reactions were started by adding the enzyme and stopped by adding 100 μL 50% (vol/vol) acetonitrile and heated at 99 °C for 1 min to pellet the protein. After centrifugation for 10 min at full speed, the samples were resolved on a Gemini C18 reverse-phase column (Phenomenex) in the following solvent gradient (solvent A, 0.2% acetic acid in water; solvent B, 0.2% acetic acid in acetonitrile): initial 5% B to 48% B at 10 min, and 11–15 min 51% B, then 16–21 min 100% B at a flow rate of 1 mL·min^{-1}. For MS analysis, we coupled an HP 1100 series II LC system (Agilent) to a Bruker Esquire ion-trap mass spectrometer (MSD trap XCT system) equipped with an ESI source. Negative ionization was attained using an ion source voltage of 3.5 kV, a corona of 4,000 nA, and a skimmer at a voltage of 40 V. Nebulization was aided by a coaxial nitrogen sheath gas at 50 psi pressure. Desolvation was ensured by a counter current nitrogen flow set at 7 psi pressure, with both the capillary and vaporizer temperature at 300 °C. Mass spectra were recorded over 15–800 *m/z* in the negative mode. K_m and V_{max} were determined by Graphpad Prism 5 software using nonlinear regression for Michaelis–Menten equation.

Accession Numbers. Sequence data from this article can be found in the GenBank/European Molecular Biology Laboratory databases under the following accession numbers: AT4G10500 (*S3H* and *SAG108*), AT3G51240 (*F3H*), AT2G14610 (*PR1*), AT1G69490 (*AtNAP*), AT5G45890 (*SAG12*), AT2G29350 (*SAG13*), AT3G48090 (*EDS1*), AT3G52430 (*PAD4*), AT1G74710 (*ICS1*) and AT1G18870 (*ICS2*), AT2G43840 (*UGT74F1*) and AT2G43820 (*UGT74F2*), AT3G11480 (*BSMT1*), AT2G23620 (*AtMES1*), AT2G23600 (*AtMES2*), AT2G23580 (*AtMES4*), AT2G23560 (*AtMES7*), and AT4G37150 (*AtMES9*).

ACKNOWLEDGMENTS. We thank Dr. Richard Amasino (University of Wisconsin-Madison) and William Gan (Cornell University) for critical readings of the manuscript and Dr. Daniel Klessig (Boyce Thompson Institute) for useful discussion. Arabidopsis Biological Resource Center (Columbus, Ohio) is thanked for sending us the T-DNA insertion mutant seed and the BAC F7L13 DNA. This research was supported by Department of Energy (DOE) Grant DE-FG02-02ER15341 and National Science Foundation (NSF) Grant MCB-0445596 (to S.-S.G.) and DOE Grant DEAC0298CH10886 (BO-147) and NSF Grant MCB-1051675 (to C.-J.L.).

1. Vlot AC, Dempsey DA, Klessig DF (2009) Salicylic acid, a multifaceted hormone to combat disease. *Annu Rev Phytopathol* 47:177–206.
2. Raskin I (1992) Role of salicylic acid in plants. *Annu Rev Plant Physiol Plant Mol Biol* 43: 439–463.
3. Zhang K, Xia X, Zhang Y, Gan SS (2012) An ABA-regulated and Golgi-localized protein phosphatase controls water loss during leaf senescence in Arabidopsis. *Plant J* 69(4): 667–678.
4. Gan S, Amasino RM (1997) Making sense of senescence: Molecular genetic regulation and manipulation of leaf senescence. *Plant Physiol* 113(2):313–319.
5. Love AJ, Milner JJ, Sadanandom A (2008) Timing is everything: Regulatory overlap in plant cell death. *Trends Plant Sci* 13(11):589–595.
6. Rivas-San Vicente M, Plasencia J (2011) Salicylic acid beyond defence: Its role in plant growth and development. *J Exp Bot* 62(10):3321–3338.
7. Dempsey DA, Vlot AC, Wildermuth MC, Klessig DF (2011) Salicylic acid biosynthesis and metabolism. *Arabidopsis Book* 9:e0156.
8. León J, Shulaev V, Yalpani N, Lawton MA, Raskin I (1995) Benzoic acid 2-hydroxylase, a soluble oxygenase from tobacco, catalyzes salicylic acid biosynthesis. *Proc Natl Acad Sci USA* 92(22):10413–10417.
9. Wildermuth MC, Dewdney J, Wu G, Ausubel FM (2001) Isochorismate synthase is required to synthesize salicylic acid for plant defence. *Nature* 414(6863):562–565.
10. Garcion C, et al. (2008) Characterization and biological function of the ISOCHORISMATE SYNTHASE2 gene of Arabidopsis. *Plant Physiol* 147(3):1279–1287.
11. Lim EK, et al. (2002) The activity of Arabidopsis glycosyltransferases toward salicylic acid, 4-hydroxybenzoic acid, and other benzoates. *J Biol Chem* 277(1):586–592.
12. Dean JV, Delaney SP (2008) Metabolism of salicylic acid in wild-type, ugt74f1 and ugt74f2 glucosyltransferase mutants of *Arabidopsis thaliana*. *Physiol Plant* 132(4):417–425.
13. Dean JV, Mohammed LA, Fitzpatrick T (2005) The formation, vacuolar localization, and tonoplast transport of salicylic acid glucose conjugates in tobacco cell suspension cultures. *Planta* 221(2):287–296.
14. Park SW, Kaimoyo E, Kumar D, Mosher S, Klessig DF (2007) Methyl salicylate is a critical mobile signal for plant systemic acquired resistance. *Science* 318(5847):113–116.
15. Zhang Z, et al. (2007) Dual regulation role of GH3.5 in salicylic acid and auxin signaling during Arabidopsis-*Pseudomonas syringae* interaction. *Plant Physiol* 145(2):450–464.
16. Bartsch M, et al. (2010) Accumulation of isochorismate-derived 2,3-dihydroxybenzoic 3-O-beta-D-xyloside in arabidopsis resistance to pathogens and ageing of leaves. *J Biol Chem* 285(33):25654–25665.
17. Friedrich L, Vernooij B, Gaffney T, Morse A, Ryals J (1995) Characterization of tobacco plants expressing a bacterial salicylate hydroxylase gene. *Plant Mol Biol* 29(5):959–968.
18. Yamamoto S, Katagiri M, Maeno H, Hayaishi O (1965) Salicylate hydroxylase, a monooxygenase requiring flavin adenine dinucleotide: I. purification and general properties. *J Biol Chem* 240(8):3408–3413.
19. Guo Y, Cai Z, Gan S (2004) Transcriptome of Arabidopsis leaf senescence. *Plant Cell Environ* 27(5):521–549.
20. Guo Y, Gan S (2006) AtNAP, a NAC family transcription factor, has an important role in leaf senescence. *Plant J* 46(4):601–612.
21. Uknes S, et al. (1992) Acquired resistance in Arabidopsis. *Plant Cell* 4(6):645–656.
22. Wisman E, et al. (1998) Knock-out mutants from an En-1 mutagenized *Arabidopsis thaliana* population generate phenylpropanoid biosynthesis phenotypes. *Proc Natl Acad Sci USA* 95(21):12432–12437.
23. Hennig J, Malamy J, Grynkiewicz G, Indulski J, Klessig DF (1993) Interconversion of the salicylic acid signal and its glucoside in tobacco. *Plant J* 4(4):593–600.
24. Morris K, et al. (2000) Salicylic acid has a role in regulating gene expression during leaf senescence. *Plant J* 23(5):677–685.
25. Buchanan-Wollaston V, et al. (2005) Comparative transcriptome analysis reveals significant differences in gene expression and signalling pathways between developmental and dark/starvation-induced senescence in Arabidopsis. *Plant J* 42(4):567–585.
26. Gan S (2010) *Plant Hormones: Biosynthesis, Signal Transduction, Action!* ed Davies PJ (Springer, Dordrecht, The Netherlands), pp 597–617.
27. Zhu S, et al. (2011) SAG101 forms a ternary complex with EDS1 and PAD4 and is required for resistance signaling against turnip crinkle virus. *PLoS Pathog* 7(11): e1002318.
28. He Y, Gan S (2002) A gene encoding an acyl hydrolase is involved in leaf senescence in Arabidopsis. *Plant Cell* 14(4):805–815.
29. Wang W, et al. (2011) Timing of plant immune responses by a central circadian regulator. *Nature* 470(7332):110–114.
30. Zhou C, Cai Z, Guo Y, Gan S (2009) An arabidopsis mitogen-activated protein kinase cascade, MKK9-MPK6, plays a role in leaf senescence. *Plant Physiol* 150(1):167–177.
31. Clough SJ, Bent AF (1998) Floral dip: A simplified method for Agrobacterium-mediated transformation of *Arabidopsis thaliana*. *Plant J* 16(6):735–743.
32. Pan X, Welti R, Wang X (2008) Simultaneous quantification of major phytohormones and related compounds in crude plant extracts by liquid chromatography-electrospray tandem mass spectrometry. *Phytochemistry* 69(8):1773–1781.
33. Thaler JS, Agrawal AA, Halitschke R (2010) Salicylate-mediated interactions between pathogens and herbivores. *Ecology* 91(4):1075–1082.
34. Zhang K, et al. (2012) An engineered monolignol 4-o-methyltransferase depresses lignin biosynthesis and confers novel metabolic capability in Arabidopsis. *Plant Cell* 24(7):3135–3152.
35. Saito K, Kobayashi M, Gong Z, Tanaka Y, Yamazaki M (1999) Direct evidence for anthocyanidin synthase as a 2-oxoglutarate-dependent oxygenase: molecular cloning and functional expression of cDNA from a red forma of *Perilla frutescens*. *Plant J* 17(2):181–189.